 CMES, vol.68, no.3, pp.269-295, 2010

# SGBEM-FEM Alternating Method for Simulating 3D Through-Thickness Crack Growth

**Jai Hak Park[1], Maan Won Kim[2] and Gennadiy P. Nikishkov[3]**

**Abstract:** A SGBEM-FEM alternating method had been proposed by Nikishkov, Park and Atluri for the analysis of three-dimensional planar and non-planar cracks and their growth. In the method, the symmetric Galerkin boundary element method is used for the crack solution in an infinite body and the finite element method is used to perform stress analysis for the uncracked body only. In this paper the method is extended further to analyze through-thickness cracks. Adequate shape of boundary element mesh is examined and it is found that the fictitious portion of the boundary element mesh, which is located outside the body, plays an important role in the method. In order to check the accuracy and efficiency of the method, the obtained stress intensity factors are compared with the known solutions or the results obtained from finite element method. Using the proposed method stress corrosion crack growth simulation is performed for a through-thickness crack with unequal surface lengths.

**Keywords:** SGBEM, FEM, alternating method, through-thickness crack, crack growth.

## 1 Introduction

For several decades the Shwartz-Neumann alternating technique has been developed for three-dimensional cracks [Atluri (1997); Atluri (2005); Nishioka and Atluri (1983), and Vijaykumar and Atluri (1981)]. Nikishkov, Park and Atluri (2001) proposed a SGBEM-FEM alternating method to analyze planar or non-planar three-dimensional cracks in a finite body. They used the symmetric Galerkin boundary element method (SGBEM) [Bonnet, Maier and Polizzotto (1998), Li and Mear (1998)] for modeling a crack embedded in an infinite body. Han and Atluri

[1] Dept. of Safety Engineering, Chungbuk National University, Chungbuk 361-763, Korea
[2] Korea Nuclear Engineering & Technology Institute, Korea Hydro & Nuclear Power Co., Daejeon 305-343, Korea
[3] Dept. of Computer Science and Engineering, The University of Aizu, Fukushima 965-8580, Japan

(2002) modified the method introducing a local finite sized subdomain. They used a crack solution in a finite subdomain instead of an infinite body using SGBEM. Until now, however, through-thickness cracks have not been considered in the alternating method. The purpose of this paper is to extend the SGBEM-FEM alternating method to obtain SIF values for a short through-thickness crack. For a long through-thickness crack, we can obtain fracture parameters using two-dimensional crack solutions. But when a through-thickness crack is short, it is impossible to use two-dimensional crack solutions because the assumptions for a two-dimensional problem are not valid. When the crack front is curvilinear or inclined to the body boundary, three-dimensional stress intensity factor (SIF) solution is necessary for fracture analysis or crack growth simulation. Well-established finite element method can be used for this purpose. But creating appropriate meshes is complicated. In this paper, the SGBEM-FEM alternating method is extended to consider a through-thickness crack problem.

In the alternating method, it can be noted [Nikishkov, Park and Atluri (2001)] that accurate solution can be obtained for a surface crack if we add a fictitious portion of the crack mesh outside the body. In this study, it is found that the fictitious portion plays a very important role in solving a through-thickness crack. And the boundary conditions imposed on the boundary element mesh also affect the solution. The effects of the fictitious portion and boundary condition are examined in this paper. The obtained SIF results are compared with the known solutions or the results obtained from finite element method. Using the developed method, stress corrosion crack growth simulation is performed for a through-thickness crack with unequal surface lengths.

## 2 SGBEM-FEM alternating method

### *2.1 Symmetric Galerkin boundary element method*

In the alternating method, a symmetric Galerkin boundary element method is used for crack modeling in an infinite body. Consider a non-planar crack of arbitrary geometry embedded in an infinite three-dimensional body. A distributed load is applied at the crack surface. The following weakly-singular boundary integral equation is valid for the crack [Bonnet, Maier and Polizzotto (1998); Xu and Ortiz (1993); Li and Mear (1998), Li, Mear and Xiao (1998)]:

$$-\int_S \int_S D_\alpha u_i^*(\mathbf{z}) C_{\alpha i\beta j}(\xi - \mathbf{z}) D_\beta u_j(\xi) dS(\xi) dS(\mathbf{z}) = \int_S u_k^*(\mathbf{z}) t_k dS(\mathbf{z}) \tag{1}$$

Here $S = S_+$ is one of crack surfaces; $u_i$ are displacement discontinuities for the crack surface; $u_i^*$ are the components of a continuous test function; and $t_k$ are crack face tractions. The weakly singular kernel $C_{\alpha i\beta j}$ is given as follows:

$$
\begin{aligned}
C_{\alpha i\beta j}(\boldsymbol{\zeta}) &= \frac{\mu}{4\pi(1-\nu)r}\left((1-\nu)\delta_{i\alpha}\delta_{j\beta}+2\nu\delta_{i\beta}\delta_{j\alpha}-\delta_{ij}\delta_{\alpha\beta}-\frac{\zeta_i\zeta_j}{r^2}\delta_{\alpha\beta}\right)\\
\boldsymbol{\zeta} &= \boldsymbol{\xi}-\mathbf{z}\\
r^2(\boldsymbol{\zeta}) &= \zeta_i\zeta_i
\end{aligned}
\tag{2}
$$

where $\nu$ is Poisson's ratio and $\mu$ is the shear modulus. Tangential operator $D_\alpha$ are defined as follows:

$$
\begin{aligned}
&D_\alpha = \frac{1}{J}\left(\frac{\partial}{\partial\eta_1}\frac{\partial x_\alpha}{\partial\eta_2}-\frac{\partial}{\partial\eta_2}\frac{\partial x_\alpha}{\partial\eta_1}\right)\\
&J = |\mathbf{s}\times\mathbf{t}|\\
&\mathbf{s} = \partial\mathbf{x}/\partial\eta_1\ ,\quad \mathbf{t} = \partial\mathbf{x}/\partial\eta_2
\end{aligned}
\tag{3}
$$

where $\eta_1$ , $\eta_2$ are the surface coordinates on the crack surface, and **s**, **t** are vectors in the plane that is tangent to the crack surface.

### *2.2 Discretization of the integral equation*

We divide the crack surface into boundary elements, and displacement discontinuities and tractions inside the elements are expressed with the values at element nodes and suitable shape functions $N_a$ as follows:

$$
\begin{aligned}
u_i &= N_a(\eta_1,\eta_2)u_{ia}\\
t_i &= N_a(\eta_1,\eta_2)t_{ia}
\end{aligned}
\tag{4}
$$

where $i$ = 1,2,3 is the global coordinate subscript; $a$ is the node number; $\eta_1,\eta_2$ are element local coordinates. Then we can rewrite the integral equation (1) in the following discretized form:

$$
-\int_S\int_S C_{\alpha i\beta j}D_\alpha N_a(z)D_\beta N_b(\xi)dS(\xi)dS(z)\,u_{jb} = \int_S N_aN_q dS(z)\,t_{iq} \tag{5}
$$

Solving Eq. (5), we can obtain the displacement discontinuities at nodes, and also can calculate stresses at inner points. It is very important to perform accurate double area integration of weakly singular kernels. Nikishkov, Park and Atluri (2001) used an efficient approach presented in references [Andra (1998); Erichsen and Sauter (1998), Frangi, Novati, Springhetti and Rovizzi (2000)]. The approach uses coordinate transformations to produce transformation Jacobian, which cancels the weak singularity of the kernel. For coincident elements and for elements with common edge or common vertex, the four-dimensional integration domain is divided into several integration subdomains. The numerical integration inside each subdomain is performed using the usual Gaussian quadrature integration rule, since all the integrals after the appropriate transformations are nonsingular [Nikishkov, Park and Atluri (2001)].

### *2.3 Alternating method*

Finite element method is well-established and widely used method for elastic and elastic-plastic structural analysis. But it is difficult to create finite element model for a body with a three-dimensional crack. The symmetric Galerkin boundary element method is a very convenient tool to solve planar or non-planar crack problems. But the matrix becomes too big when considering complex geometry and boundary elements for a crack are coupled with boundary elements for a body. A SGBEM-FEM alternating method is a method to employ advantages of both methods. The method obtains the solution for a finite body with a crack as a superposition of two models:

- finite element model for a finite body under external loading, without a crack;
- an infinite body with a crack modeled by the symmetric Galerkin boundary element method.

Because the crack is not included in the finite element model, its creation is easy. And because the SGBEM is used to obtain the solution for a crack in an infinite body, the boundary element mesh is independent of the body and can be changed easily during the crack growth.

The basic steps of the SGBEM-FEM alternating iteration procedure are as follows:

1. Using the FEM, obtain the stresses at the location of the crack in a finite uncracked body subjected to given boundary conditions.
2. Using the SGBEM, solve the problem for the crack, faces of which subjected to tractions, found from FEM analysis of the uncracked body.
3. Determine the residual forces at the outer boundaries of the finite body, from displacement discontinuities at the crack surface.
4. Using the FEM, solve a problem for the finite uncracked body under residual forces from SGBEM analysis.

5. Obtain the stresses at the location of the crack corresponding to FEM solution.

6. Repeat Steps (2)-(5) until the residual load becomes small enough.

7. By accumulating all the appropriate contributions, compute the total solution for a finite body with the crack.

### *2.4 Calculation of fracture mechanics parameters*

Once the displacement discontinuities are obtained at nodes, the stress intensity factors $K_I$, $K_{II}$ and $K_{III}$ can be easily determined using the following relations:

$$\begin{aligned} K_I &= \frac{E\sqrt{\pi}}{(1-\nu^2)}\frac{u_3}{4\sqrt{2r}} \\ K_{II} &= \frac{E\sqrt{\pi}}{(1-\nu^2)}\frac{u_2}{4\sqrt{2r}} \\ K_{III} &= \frac{E\sqrt{\pi}}{(1+\nu)}\frac{u_1}{4\sqrt{2r}} \end{aligned} \tag{6}$$

where $K_I$, $K_{II}$ and $K_{III}$ are the stress intensity factors; $E$ is the elasticity modulus; $\nu$ is the Poisson's ratio; $r$ is the distance from the point to the crack front and $u_1$, $u_2$ and $u_3$ are components of the displacement discontinuities at points at the crack surface in a local crack front coordinate system, $x_1$, $x_2$ and $x_3$. The axis $x_1$ of the crack front coordinate system is parallel to the crack front, and the axis $x_3$ is normal to the crack surface.

The following procedure for the stress intensity factor calculation is used in the current work:

1. Obtain the displacement discontinuities $u_i^G$in the global coordinate system for the quarter-point node and for the corner node of a singular crack front element;

2. Extrapolate $u_i^G/\sqrt{r}$ to the crack front, using values at the quarter-point node $(L/4)$ and at the corner node $(L)$. Here $r$ is the distance along line normal to the crack front and $u_i^G$components of displacement discontinuities in the global coordinate system.

3. Transform the extrapolated displacement discontinuities from the global coordinate system to the crack front coordinate system, $u_i = \alpha_{ij}u_i^G$ where $\alpha_{ij}$ are direction cosines of the transformation.

4. Calculate the stress intensity factors using equation (6).

When a crack front element edge is not normal to the crack front, a modification of the obtained SIF is necessary. Let consider a crack front element with an inclined element edge as shown in Fig. 1. AB is a part of crack front. If we calculate mode I SIF along the edge AD using Eq. (6), the obtained SIF is the following $K_I'$ instead of $K_I$.

$$K_I' = \frac{E\sqrt{\pi}}{(1-\nu^2)} \frac{u_3}{4\sqrt{2r'}} \tag{7}$$

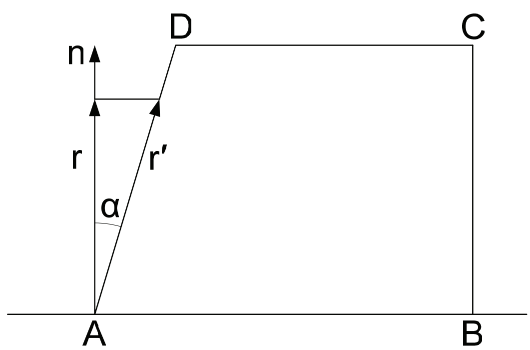


Figure 1: A crack front element with an inclined element edge.

Here $r'$ is the distance from the point A. Since $r = r' \cos\alpha$, we can obtain the following relation:

$$K_I = \frac{E\sqrt{\pi}}{(1-\nu^2)} \frac{u_3}{4\sqrt{2r}} = \frac{K_I'}{\sqrt{\cos\alpha}} \tag{8}$$

Equation (8) is satisfied when SIF is constant along the crack front. But it can be used when SIF variation is not much along the crack front.

## 3 Modeling crack growth

### *3.1 Modeling of non-planar crack growth*

SGBEM-FEM alternating method is quite suitable for crack growth simulation. Since the crack is modeled separately, the finite element model need not be modified during crack growth. Only the boundary element model (crack model) should

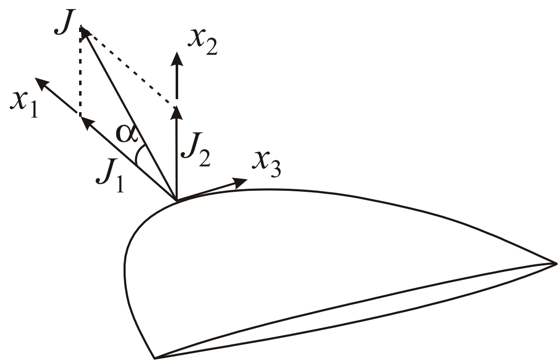


Figure 2: Components $J_1$ and $J_2$ of the $J$-integral at the crack front. It is supposed that the crack grows in the direction of the $J$-integral.

be changed during crack growth. For crack growth simulation of a non-planar crack, it is necessary to know the direction of crack growth and the amount of crack growth. The $J$-integral is used to determine the crack growth direction and the amount of crack growth as follows:

- Crack grows in the direction of $J$-integral vector as shown in Fig. 2;
- Crack growth rate is determined by the effective stress intensity factor $K_{eff}$ based on the $J$-integral.

In an elastic three-dimensional case, the $J$-integral components are evaluated using the stress intensity factors as:

$$\begin{aligned} J_1 &= \frac{1-\nu^2}{E}(K_I^2 + K_{II}^2) + \frac{1+\nu}{E}K_{III}^2 \\ J_2 &= -2\frac{1-\nu^2}{E}K_I K_{II} \\ J &= \sqrt{J_1^2 + J_2^2} \end{aligned} \tag{9}$$

where $E$ is the elasticity modulus and $\nu$ is the Poisson's ratio. The crack growth angle $\alpha$, which is the angle between the axis $x_1$ and the crack growth direction, is determined by the direction of $J$-integral vector:

$$\tan\alpha = \frac{J_2}{J_1} \tag{10}$$

It is worth noting that the $J$-integral vector is normal to the crack front. Hence a point at the crack front moves in the plane normal to the crack front at the angle $\alpha$, from the plane which is tangential to the crack surface.

Typical crack growth model, suitable for fatigue or SCC crack growth simulation can be expressed using the effective stress intensity factor $K_{eff}$ as follows:

$$\frac{da}{dt} = f(K_{eff}) \tag{11}$$

where *da/dt* is the crack growth rate and $K_{eff}$ is related to the $J$-integral as:

$$K_{eff} = \sqrt{\frac{JE}{1-\nu^2}} \tag{12}$$

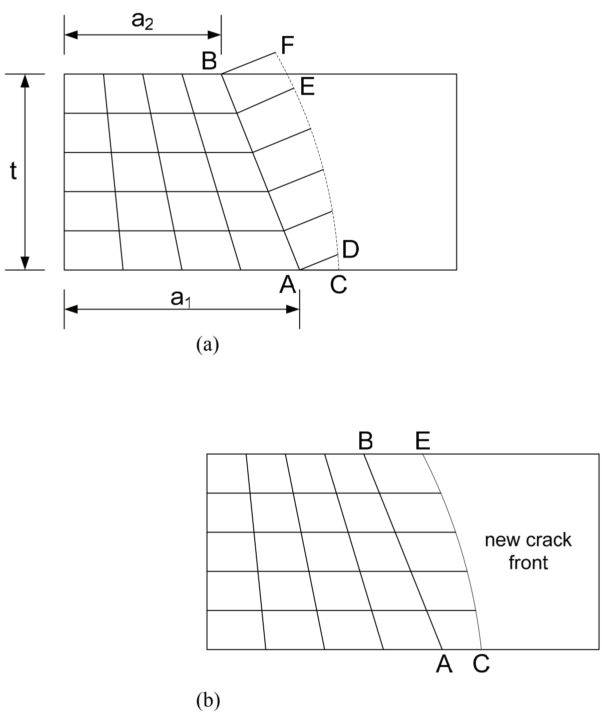


Figure 3: Crack growth model for a through-thickness crack: (a) Advance location of current crack front points (b) Crack mesh after adding new crack front element layer.

### 3.2 Crack growth algorithm

The following algorithm is used to model mixed mode SCC crack growth.

1. Solve the boundary value problem for the current crack configuration using the SGBEM-FEM alternating method.

2. Obtain the stress intensity factors $K_I$, $K_{II}$ and $K_{III}$ for the element corner nodes located at the crack front and calculate the effective stress intensity factor $K_{eff}$ according to Equation (12) and select the maximum value $K_{eff}^{\max}$.

3. Estimate increment of the crack life by the following integration and accumulate the crack life $t = t + \Delta t$:

$$\Delta t = \int_a^{a+\Delta a} \frac{da}{f(K_{eff}(a))} \tag{13}$$

4. If no value of crack advance $\Delta a_{mac}$ is left in the input data then stop.

5. For each corner node determine the crack front coordinate system by averaging the coordinate axis vectors determined at the corner point of two neighboring boundary elements. Also determine $X_1$, $X_2$ and $X_3$ coordinate system. The $X_3$ axis is normal to the crack surface and the $X_1 - X_2$ plane coincides with the crack surface. In addition the $X_1$ axis is parallel to the side surface of the body near the crack front.

6. For each corner node, calculate the crack growth angle $\alpha$ according to Equation (10).

7. Determine crack advance $\Delta a$ for the corner nodes at the crack front using the following equation:

$$\Delta a = \Delta a_{\max} \frac{f(K_{eff})}{f(K_{eff}^{\max})} \tag{14}$$

8. Move the corner nodes along the $J$-integral vector according to computed $\Delta a$ values. Some nodes can be located outside the body as shown in Fig. 3(a).

9. Transform the coordinates of the advance nodes in the $X_1$, $X_2$ and $X_3$ coordinate system. Perform curve fitting for $X_1$ and $X_3$ coordinates with respect to $X_2$ coordinate using a polynomial expression.

10. It is assumed that the crack front nodes advance preserving their $X_2$ coordinates. Using the fitting polynomial, obtain the $X_1$ and $X_3$ coordinates of advance points as shown in Fig. 3(b). The curve CE in Fig. 3(b) becomes new crack front.

11. For the crack front points located outside the body, we use the same $\Delta a$ and $\alpha$ as the values calculated at the nearest crack front point on the body boundary.

12. Find the locations of crack front midside nodes, using linear or cubic spline interpolation.

13. Shift the quarter-point nodes of the previous crack front elements to midside position. Put quarter-point nodes on element sides nearly normal to the crack front.

14. Generate one layer of boundary elements between old and new crack fronts.

15. Go to step (1)

### *3.3 Crack front smoothing*

When crack growth simulation is performed using the alternating method, oscillation phenomenon is observed in crack advance and SIF distribution. The phenomenon occurs due to the following reason. If a crack front point advances less than adjacent crack front points due to calculation error or local geometry, the SIF of the point becomes larger than the values of adjacent crack front points. So in the next increment, the crack front point advances more than other adjacent points. Then after the increment, the SIF of the point becomes less than other points. If oscillating amplitude in SIF or crack advance does not decrease during next increment steps, the crack growth simulation fails.

To prevent the oscillation phenomenon, geometrical smoothing can be used. The step (10) in crack growth algorithm in section 3.2 implies the geometrical smoothing. Figure 4 illustrates the procedure of geometrical smoothing. Let consider a procedure to find a new advancing crack front point $A'$ corresponding to the current crack front point $A$. First obtain the crack advance points corresponding to the current crack front points. The open circles in Fig. 4 denote the crack advance points. After transforming the coordinates of the points in the $X_1$, $X_2$ and $X_3$ coordinate system, curve fitting is performed for $X_1$ and $X_3$ coordinates with respect to $X_2$ coordinate using a polynomial expression. Let the number of points used in the curve fitting be $n_{fit}$. An even $n_{fit}$ value can remove the oscillating phenomena more effectively than an odd $n_{fit}$ value. In this study, the second order polynomial is used in curve fitting and $n_{fit}$ = 6 is used. Using the obtained fitting polynomials, the $X_1$ and $X_3$ coordinates of $A'$ can be calculated easily.

In usual SIF distribution obtained from alternating method, the SIF value at the body boundary is less than the value inside the body. If we use the SIF values at the boundary in crack growth simulation without modification, it may be the source of the oscillation phenomenon. Instead of the obtained SIF value, extrapolated SIF value using inner 2 or 3 points can be used. It is also possible to perform crack front geometrical smoothing excluding the front points on the body boundary. In the case, the obtained SIF value on the body boundary is not used.

### 3.4 Crack growth material model

Several material models for determining the SCC crack growth rate in the stainless steel-water systems has been developed [Saito and Kuniya (2001); Peng, Kwon and Shoji (2004)]. Currently for testing the developed crack growth procedure, we use the mechanochemical model proposed by Saito and Kuniya (2001). The model is represented by the following equation:

$$\frac{da}{dt} = A_0 \left[ C_1 \exp\left(-C_2 \left(C_3 - C_4 (K_{eff} - K_{ISCC})\right)\right)^{2/(n+1)} \right]^m \tag{15}$$

Here $K_{eff}$ is the effective stress intensity factor calculated through the $J$-integral value,$A_0$, $C_1$, $C_2$, $C_3$, $C_4$ are material constants, $K_{ISCC}$ is the threshold stress intensity factor, $n$ is the Ramberg-Osgood type strain hardening coefficient, $m$ is the parameter representing the effect of environment and material chemistry.

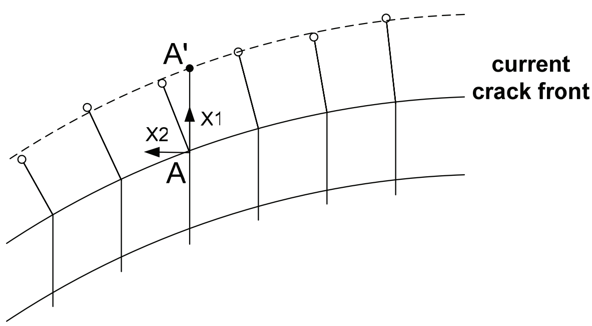


Figure 4: Crack front smoothing

## 4 Through-thickness crack

Typical boundary element mesh used for a through-thickness crack with different surface lengths is shown in Fig. 5. In the figure, $t$ is the thickness of a body and

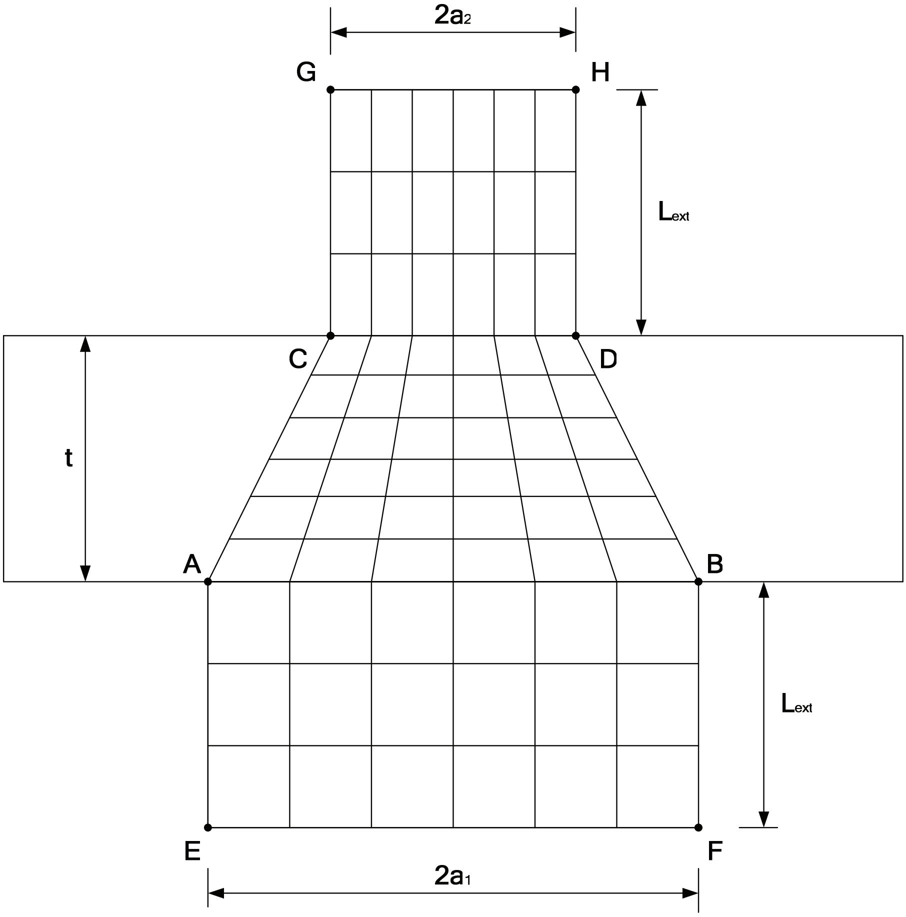


Figure 5: Boundary element mesh for a through-thickness crack.

$2a_1$, $2a_2$ are the crack lengths on the surface. Quadrilateral ABDC is the region embedded in the body and other regions in the mesh are located outside the body. Let $L_{ext}$ be the length of the outside mesh as shown in Fig. 5. In Fig. 5, all edges except EF and GH are assumed as crack fronts. So zero crack opening displacement (COD) condition is applied on all edges except EF and GH. The boundary conditions imposed on the edges EF and GH also affect the solution.

When free boundary conditions are imposed on EF and GH, finite value of COD is obtained along EF and GH. Since COD must be zero outside the boundary element mesh, finite value of COD is physically incompatible state. If the length $L_{ext}$ is very

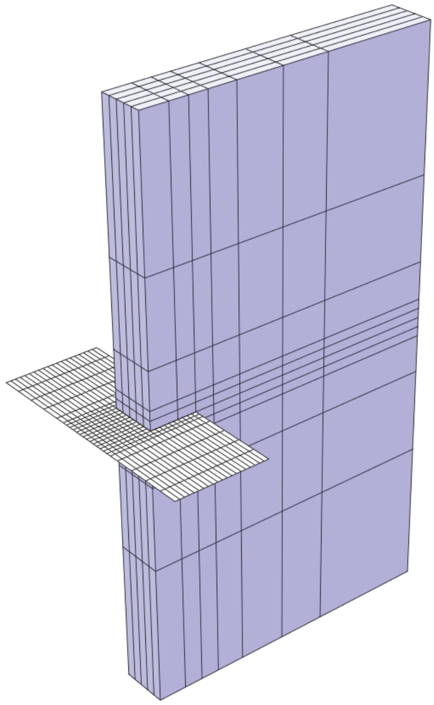

Figure 6: Example of a finite element mesh and boundary element mesh (crack mesh) used in the study. Only the half of the finite element mesh is plotted.

short, large COD is obtained along EF and GH and incorrect large SIF are obtained along crack front. If the length $L_{ext}$ is long, the COD on EF and GH is small and the obtained SIF is nearly the same as the case when zero COD condition is imposed along EF and GH.

### 4.1 Effect of $L_{ext}$

A simple problem is considered to examine the effect of $L_{ext}/t$ on SIF of a through-thickness crack. A through-thickness crack with surface length $2a$ is located at the center of a plate. The width, thickness and height of the plate are 0.64 m, 0.05 m, 0.6 m respectively and normal stress $\sigma$=100 MPa is applied on the edge surfaces of the body. The material of the body is assumed as an elastic material with elastic modulus $E$= 210 GPa and Poisson's ratio $\nu$=0.3. Figure 6 shows an example of finite element mesh and boundary element mesh (crack mesh). Only a half of finite element mesh is plotted. In the finite element model, 3639 nodes and 700 20-node

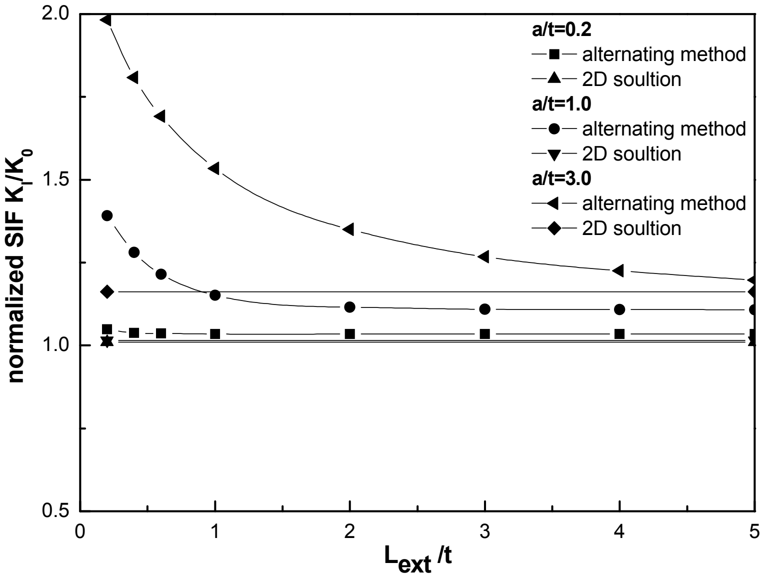


Figure 7: Effect of $L_{ext}$ on the normalized stress intensity factors when free boundary condition is imposed on the edges EF and GH in Fig. 6.

three-dimensional solid elements are used and in the crack mesh, 1529 nodes and 480 8-node boundary elements are used. To represent stress singularity at the crack front, the midside nodes are moved to the quarter positions in crack front elements. The smallest element size in the mesh shown in Fig. 6 is 0.005m×0.005m. The run time is 580 sec on an Intel 3 MHz personal computer for the typical model in Fig. 6. The SIF is the value at the center of the thickness normalized by $\sigma\sqrt{\pi a}$. For comparison, the two-dimensional solutions are also plotted.

The maximum SIF value on the crack front of a through-thickness is larger than the two dimensional SIF solution. According to the result in Okada and Kamibeppu (2005), the maximum SIF value is about 10% larger than the two-dimensional solution. According to the results given in Murakami (1987), the maximum SIF value depends on the Poisson's ratio $\nu$. In the given solution for $\nu$=0.3, the maximum SIF value is about 4% larger than the two-dimensional solution in an infinite plate.

Figure 7 shows the effect of $L_{ext}/t$ on SIF of a through-thickness crack. Free boundary condition is imposed on the edges EF and GH in Fig. 5. When $a/t$=0.2, the effect of $L_{ext}/t$ is very small. The normalized SIF value remains nearly constant regardless of $L_{ext}/t$ value. And the constant value is nearly the same as the two-dimensional solution. The value is about 2% larger than the two-dimensional solution. So when the crack length is short compared to the thickness, accurate SIF value can be obtained regardless of $L_{ext}/t$ value. When $a/t$=1.0, the SIF value obtained from the alternating method varies according to $L_{ext}/t$ value. When $L_{ext}/t$ is small, the SIF value is much larger than the two-dimensional solution. As $L_{ext}/t$ increases, the SIF value decreases to a constant value, which is about 9% larger than the two-dimensional solution. So in order to obtain the converged solution, $L_{ext}/t$ should be greater than 2. If $L_{ext}/t$ is less than 2, the obtained SIF is greater than the converged solution. When $a/t$=3.0, the SIF value obtained from the alternating method is much larger than the two-dimensional solution when $L_{ext}/t$ is small. As $L_{ext}/t$ increases, the SIF value converges to a constant value. When $L_{ext}/t$= 5, the obtained SIF value is not fully converged and 1.3% larger than the two-dimensional solution.

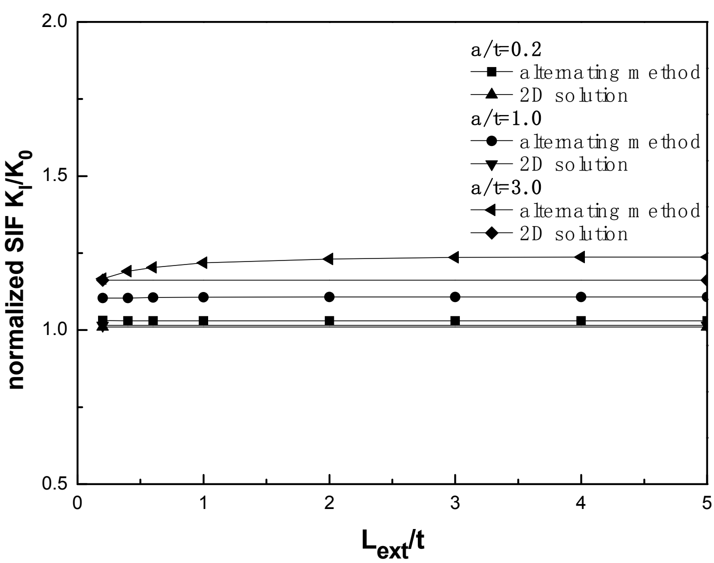


Figure 8: Effect of $L_{ext}$ on the normalized stress intensity factors when zero COD boundary condition is imposed on the edges EF and GH in Fig. 6.

Next, the effect of $L_{ext}/t$ on SIF of a through-thickness crack is examined when zero COD boundary condition is imposed on the edges EF and GH in Fig. 5. In Fig. 8, the variation of the normalized SIF valued is plotted as a function of $L_{ext}/t$ when

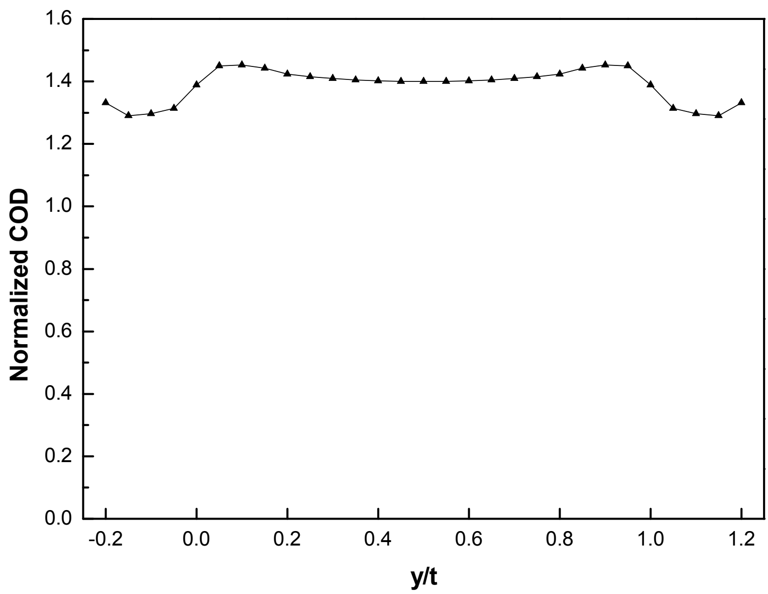


Figure 9: Normalized COD distribution along vertical center line of the crack mesh when free COD boundary condition is imposed on the edges EF and GH in Fig. 6. Here $a/t$=1, $L_{ext}/t$=0.2 and COD is normalized by $4\sigma a/E$.

$a/t$=0.2, 1.0 and 3.0 respectively. For comparison, the two-dimensional solutions are also plotted in the figure. When $a/t$=0.2 and 1.0, the SIF shows a constant value regardless of $L_{ext}/t$. The effect of $L_{ext}/t$ is observed only when $a/t$=3.0 and $L_{ext}/t$ is less than 1. So if the zero COD boundary condition is used, converged SIF solution can be obtained when we use $L_{ext}/t$ value greater than 1.

In order to examine the reason of the effect of the boundary condition imposed on crack mesh edges, COD is calculated along vertical center line of crack mesh. Figure 9 shows normalized COD distribution along vertical center line of the crack mesh when free COD boundary condition is imposed on the edges EF and GH in Fig. 6. Here $a/t$=1, $L_{ext}/t$=0.2 and COD is normalized by $4\sigma a/E$, which is the maximum COD in two dimensional solution. It can be noted that COD has finite value at the points on crack mesh edge, i.e. at the points with $y/t$= -0.2 and 1.2. Physically COD must be zero at the points on crack mesh edge. We obtained large COD value compared two-dimensional COD solution. That is the reason why large SIF is obtained when small $L_{ext}/t$ value is used. Figure 10 shows normalized COD

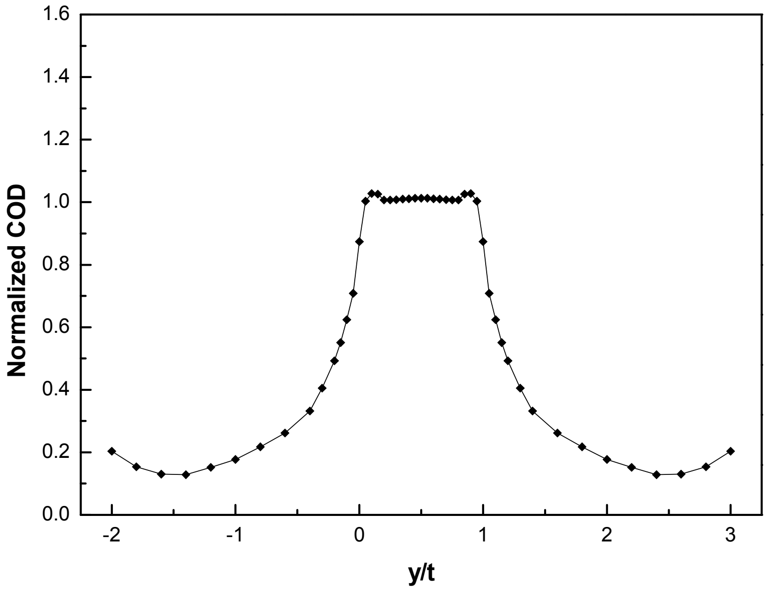


Figure 10: Normalized COD distribution along vertical center line of the crack mesh when free COD boundary condition is imposed on the edges EF and GH in Fig. 6. Here $a/t$=1, $L_{ext}/t$=2 and COD is normalized by $4\sigma a/E$.

distribution along vertical center line of the crack mesh when free COD boundary condition is imposed on the edges EF and GH in Fig. 5. Here $a/t$=1, $L_{ext}/t$=2. COD shows small value near the crack mesh edge. That is why we obtain converged solution when large $L_{ext}/t$ value is used.

Next, normalized COD distribution is obtained along vertical center line of the crack mesh when zero COD boundary condition is imposed on the edges EF and GH in Fig. 5. Figures 11 and 12 show the results when $L_{ext}/t$=0.2 and 2 respectively. Nearly the same maximum COD values are obtained regardless of $L_{ext}/t$ value.

### *4.2 Effect of boundary element mesh*

We examined the effect of boundary element mesh on the SIF distribution of a through-thickness crack in a plate. The length of a through-thickness crack is $2a$ = 0.1 m and the dimensions of the plate is same as in the previous problem. It is

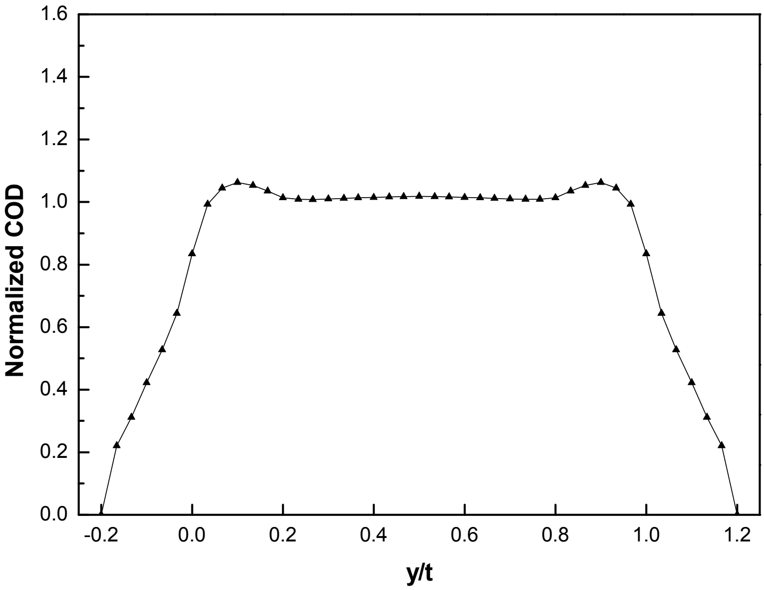


Figure 11: Normalized COD distribution along vertical center line of the crack mesh when zero COD boundary condition is imposed on the edges EF and GH in Fig. 6. Here $a/t$=1, $L_{ext}/t$=0.2 and COD is normalized by $4\sigma a/E$.

adopted that $L_{ext}/t$= 2 in the boundary element mesh. Four kinds of meshes are used. The smallest element size of the coarsest mesh is 0.01 m $\times$ 0.01 m and the size of the finest mesh is 0.0025 m $\times$ 0.0025 m. Figure 13 shows boundary element mesh with size of 0.00333 m $\times$ 0.00333 m. The shaded region ABDC is the region located inside the body, and other regions are located outside the body.

A simple definition of a quality of a quadrilateral element is $Q = h_{\max}/h_{\min}$. Here $h_{\max}$ and $h_{\min}$ are the smallest and the largest edges in the element. Best results can be obtained when the element quality is equal to 1. But in order to reduce calculation time, we have to reduce the number of boundary elements. From the experience, it is noted that the element quality can be 2 or 3 in the boundary element region embedded in the body, i.e., the shaded region in Fig. 9. And the element quality can be 5 or 6 in the boundary element region outside the body. But as shown in Fig. 9, the element quality in the region near AB or CD should be same as in the inside region and the quality can increase as the region goes farther from AB or CD.

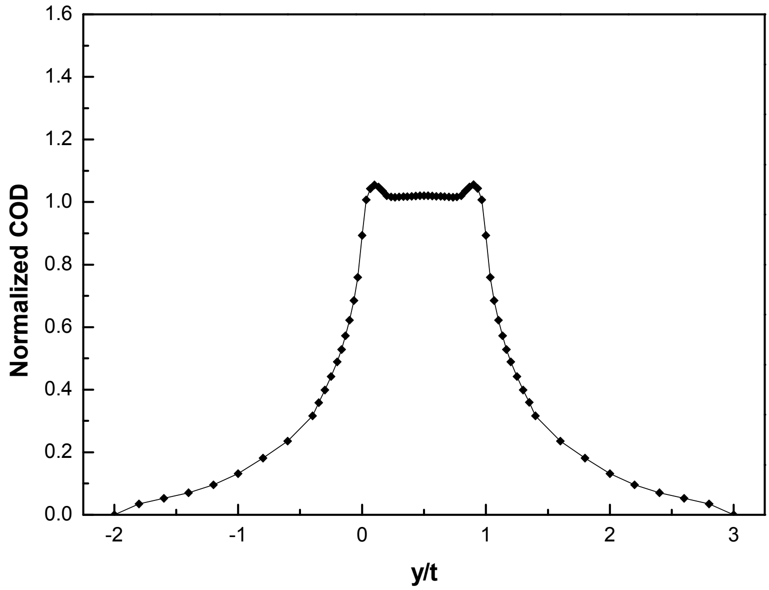


Figure 12: Normalized COD distribution along vertical center line of the crack mesh when zero COD boundary condition is imposed on the edges EF and GH in Fig. 6. Here $a/t$=1, $L_{ext}/t$=2 and COD is normalized by $4\sigma a/E$.

The obtained SIF distributions are given in Fig. 14. The SIF is normalized by $\sigma\sqrt{\pi a}$. Normalized SIF distribution is given as a function of $y/t$. Here $y$ is the coordinate in the through-thickness direction. In every distribution, the maximum SIF value is obtained at the center of the thickness and SIF shows the minimum value at the body boundary. Besides the coarsest mesh, all other 3 types of meshes give nearly the same SIF distribution. And the maximum SIF value shows about 10% larger value than the two-dimensional solution. The distribution shape and the maximum value are consistent with the results obtained using virtual crack closure-integral method (Okada and Kamibeppu, 2005).

### *4.3 Through-thickness crack with unequal surface lengths*

SIF distribution is obtained for a through-thickness crack with unequal surface lengths using the SGBEM-FEM alternating method. Let the surface lengths of the crack be $2a_1$, $2a_2$ and let initial crack front be straight as shown in Fig. 5.

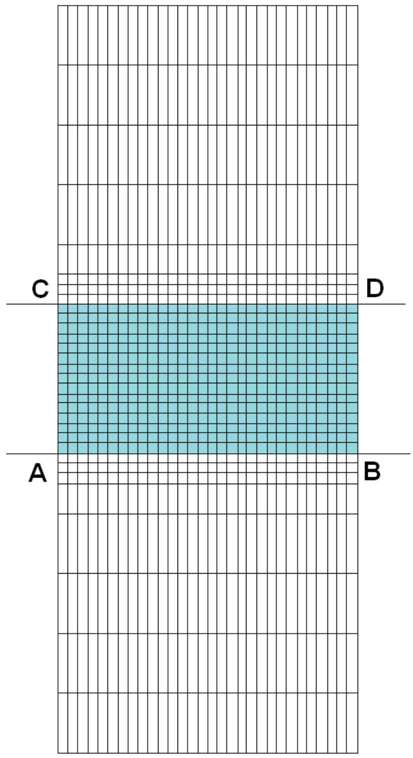


Figure 13: Example of boundary element mesh (0.00333 m × 0.00333 m)

Three crack geometries are considered. Three cracks have the same $a_1$ value of 0.05 m, but different $a_2$ values of 0.05 m, 0.04 m and 0.025 m respectively. An example of boundary element mesh used for the crack with $a_2$=0.025 m is shown in Fig. 15. For comparison, SIF values are also obtained using finite element method. A commercial code, ABAQUS is used in the analysis (ABAQUS, 2010). ABAQUS code provides several convenient commands for modeling a crack, and SIF values are obtained using the J-integral values for contours surrounding the crack front. In the finite element model, 4704 20-node elements and 21848 nodes are used. The used finite element model for $a_2$=0.025 m is illustrated in Fig. 16.

The SIF distributions along the crack front are given in Fig. 17. For the crack with $a_2$=0.05 m, symmetric SIF distribution is obtained and the maximum SIF value occurs at the middle of the thickness. For the crack with $a_2$=0.04 m, the SIF value near $a_1$ is lower than the SIF value near $a_2$. Here the point with $y/t$=0 corresponds

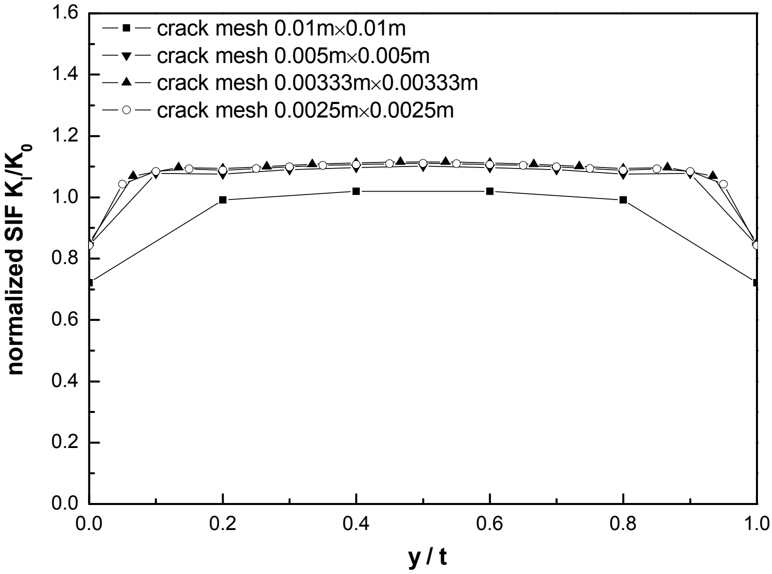


Figure 14: Effect of boundary element meshes on the stress intensity factor distribution along the thickness.

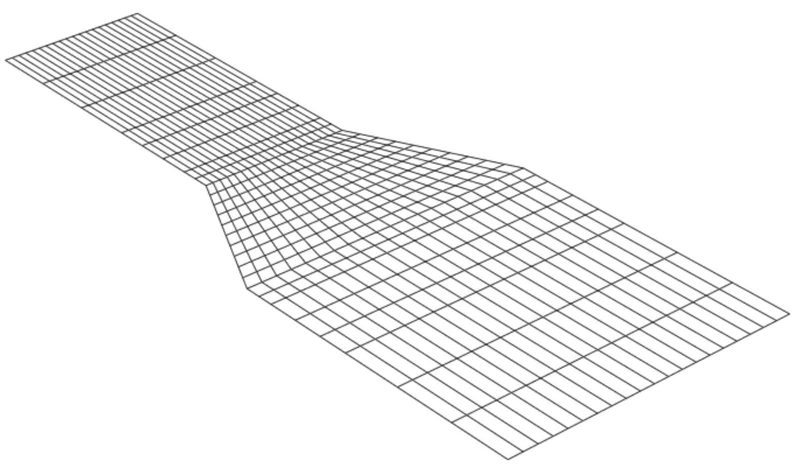

Figure 15: Boundary element mesh for a through-thickness crack with unequal surface lengths

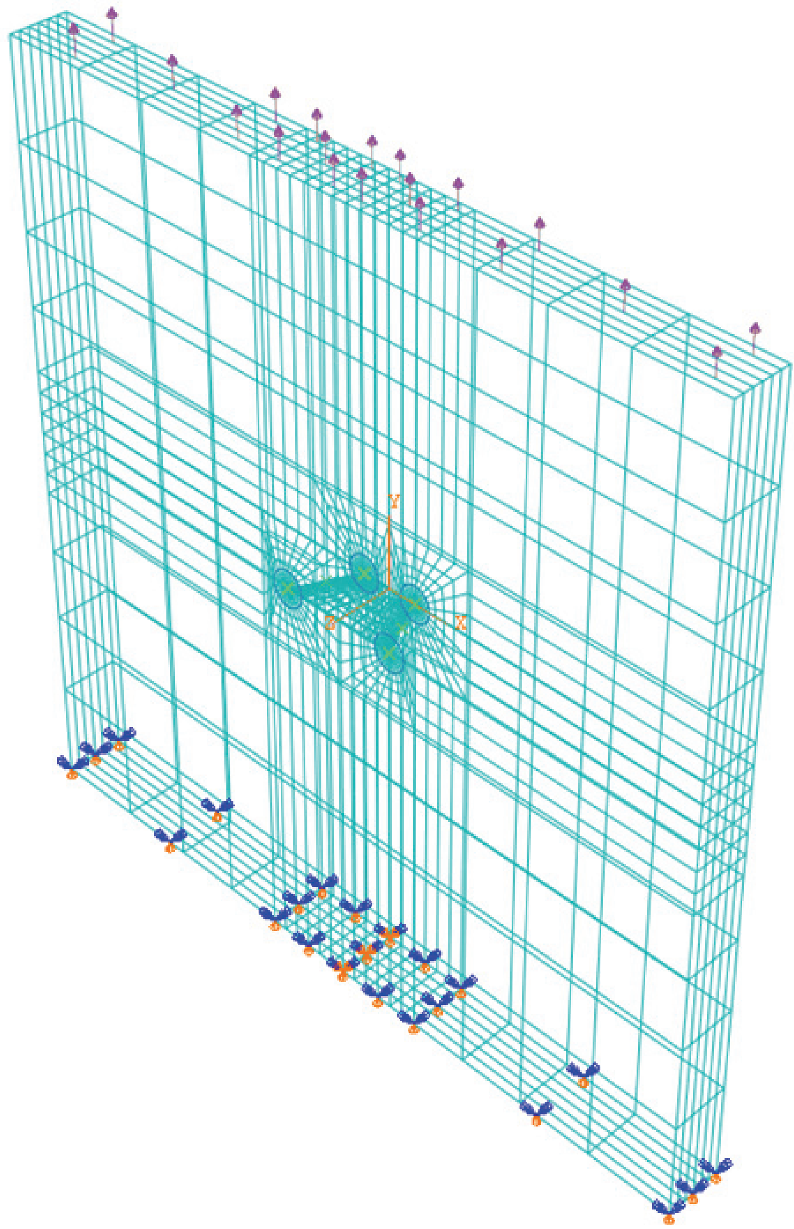


Figure 16: A finite element model for $a_1$=0.05m and $a_2$=0.025m.

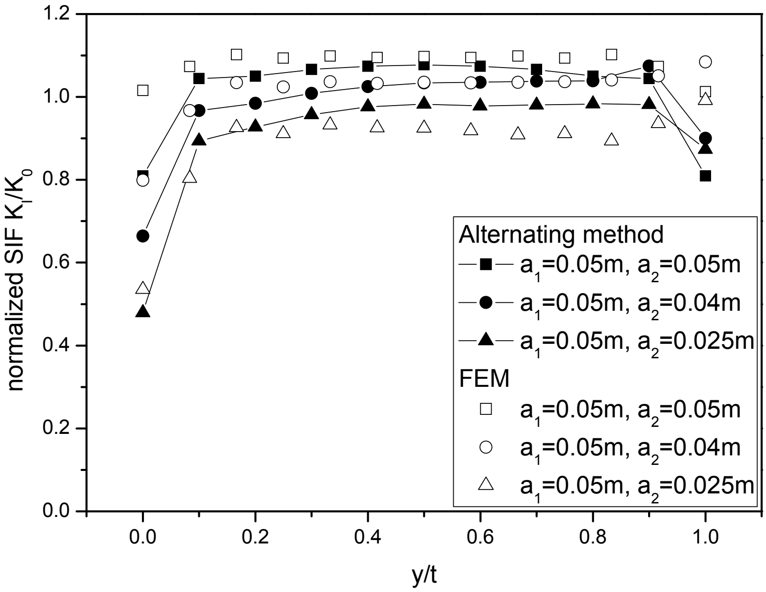


Figure 17: SIF distribution for a through-thickness crack with unequal surface lengths.

to $a_1$ and the point with $y/t$=1 corresponds to $a_2$. The maximum SIF value occurs at the first inner point near $a_2$. The maximum value, however, is less than the maximum value for the crack with $a_2$=0.05 m. The two-dimensional SIF solution for $a$=0.04 m is 35.8 MPa $m^{1/2}$. So the SIF value at the first inner point near $a_1$ is about 7% larger than the two-dimensional SIF solution. For the crack with $a_2$=0.025 m, the SIF value near $a_1$ is also lower than the SIF value near $a_2$. And the maximum SIF value is lower than the maximum value of the crack with $a_2$=0.04 m. The two-dimensional SIF solution for $a$=0.025 m is 18.1 MPa $m^{1/2}$. And the SIF value at the first inner point near $a_1$ is 35.4 MPa $m^{1/2}$, which is much larger than the two dimensional SIF value. For a through-thickness crack with unequal surface lengths, it is noted that the SIF corresponding to the shorter surface length is larger than the SIF for the longer surface length.

Figure 17 also shows the comparison between two results obtained from alternating method and finite element method. The open symbols in Fig. 17 denote the SIF values obtained using finite element method. Excluding the points on the free surface, similar SIF values are obtained for the cases of $a_2$=0.05 m and $a_2$=0.04 m.

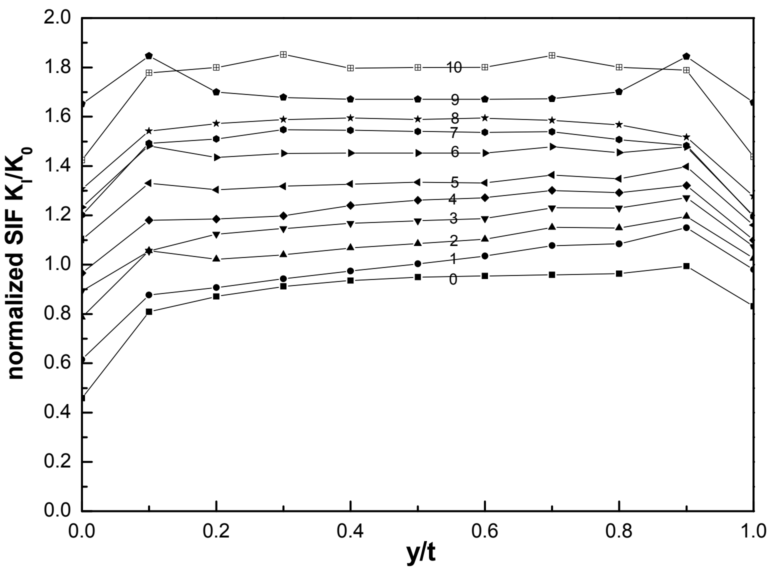


Figure 18: Stress intensity factor $K_I$ for a through-thickness crack during stress corrosion crack growth.

But large discrepancy is observed when $a_2$=0.025. Excluding the points on the free surface, the SIF values from alternating method are larger than those from finite element method. We cannot say that the result from finite element method is more accurate than the results from alternating method. More rigorous and careful finite element analysis seems to be necessary to obtain correct SIF values.

### *4.4 Crack growth*

Crack growth simulation is performed starting from a through-thickness crack with unequal surface lengths subject to uniform tensile loading. The surface crack lengths of the crack are $a_1$=0.05 m and $a_2$=0.025 m, the applied loading is $\sigma$=100MPa and the material and the geometry of the body are the same as the previous problem. The initial boundary element mesh is nearly the same as the mesh illustrated in Fig. 15 except the length $L_{ext}$. In this simulation, $L_{ext}/a_1$=6 is used. The SCC material model of Eq. (15) is used with the parameters $A_0$=$1.1\times10^{-7}$, $C_1$=$2.5\times10^{10}$, $C_2$=12.9199, $C_3$=3.0, $C_4$=0.15, $K_{ISCC}$=9.0 MPa m$^{1/2}$ and $n$=5. The crack growth algorithm described in section 3.2 is used. Ten crack advancements are performed.

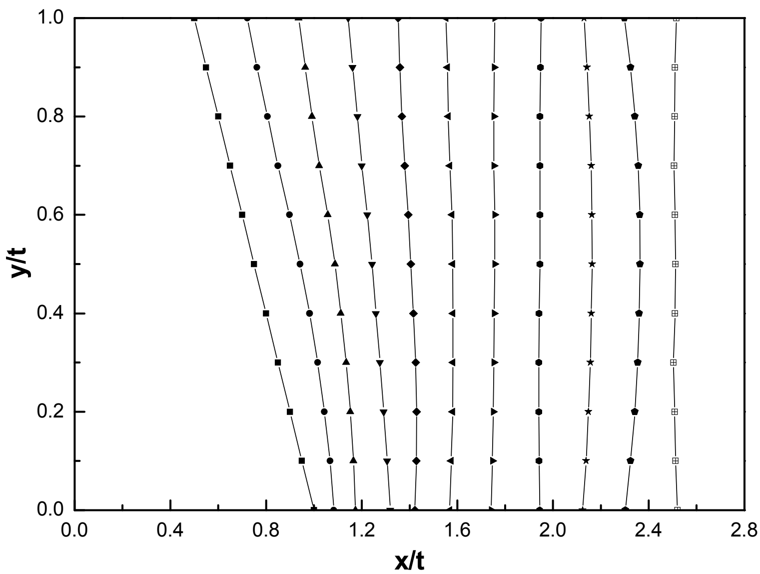


Figure 19: Crack fronts during crack growth for a through-thickness crack

The maximum specified increment, $da_{max}$ is 0.01 m in each advance except the $8^{th}$ advance, where $da_{max}$ is 0.011 m.

Figure 18 shows SIF distribution after crack increments. For the initial crack, the SIF near long crack length is lower than the SIF near short crack length. As the crack grows, SIF distribution becomes symmetric. SIF values on the boundary are not used in the simulation, because the crack front smoothing is performed excluding the crack front points on the boundary. Figure 19 shows crack fronts during the stress corrosion crack growth.

The accuracy and computational stability depends on the maximum specified increment, $da_{max}$. If inadequate increment value is specified, a crack element with poor quality is generated during the crack growth simulation. And the simulation fails because of inaccurate SIF value.

## 5 Conclusion

The SGBEM-FEM alternating method is extended to model a through-thickness three-dimensional crack in a finite body. The symmetric Galerkin boundary element method is used to obtain the solution for a crack in an infinite medium. A body without a crack is modeled by the finite element method. It is found that the fictitious portion of boundary element mesh (crack mesh) plays an important role in solving a through-thickness crack. The effect of the length of the fictitious portion on SIF solution is examined. The effect of the boundary condition imposed on crack mesh edges is also examined. It is noted that as the length of the fictitious portion increases the SIF converges to a constant value. When zero COD boundary condition is imposed on the crack mesh edges, a converged solution can be obtained with shorter length of the fictitious portion compared to the free boundary condition.

The accuracy and efficiency is examined by solving example problems for through-thickness cracks with equal and unequal surface lengths. Stress corrosion crack growth simulation is also performed using the developed SGBEM-FEM alternating method. It is found that the developed SGBEM-FEM alternating method can be used as an effective method to analyze a short through-thickness crack in a finite body.

## References

**ABAQUS** standard manual, V.6.10, 2010.

**Andra, H.** (1998): Integration of singular integrals for the Galerkin-type boundary element method in 3D elasticity. *Comp. Methods Appl. Mech. Engng*, vol. 157, pp. 239-249.

**Atluri S.N.** (1997): *Structural Integrity and Durability*, Tech Science Press, Forsyth.

**Atluri S.N.** (2005): Applications of DTALE: Damage Tolerance Analysis and Life Enhancement [3-D Non-plannar Fatigue Crack Growth], *Structural Integrity & Durability*, vol. 1, no. 1, pp. 1-20.

**Bonnet, M.; Maier, G.; Polizzotto, C.** (1998) Symmetric Galerkin boundary element methods. *Appl. Mech. Rev.*, vol. 51, pp. 669-704.

**Erichsen, S.; Sauter, S.A.** (1998): Efficient automatic quadrature in 3-d Galerkin BEM. *Com. Methods Appl. Mech. Engng*, vol. 157, pp. 215-224.

**Frangi, A.; Novati, G.; Springhetti, R.; Rovizzi, M.** (2000): Fracture mechanics in 3D by the symmetric Galerkin boundary element method. *VIII Conf. On Numerical Methods in Continuum Mechanics, 19-24 Sept. 2000, Liptovsky Jan, Slovak Republic*.

**Han, Z.D.; Atluri, S.N.** (2002): SGBEM (for cracked local subdomain)-FEM (for uncracked global structure) alternating method for analyzing 3D surface cracks and their fatigue-growth, *CMES: Computer Modeling in Engineering & Sciences*, vol.

3, no. 6, pp. 699-716.

**Li, S.; Mear, M.E.** (1998): Singularity-reduced integral equations for displacement discontinuities in three-dimensional linear elastic media. *Int. J. Fract.*, vol. 93, pp. 87-114.

**Li, S.; Mear, M.E.; Xiao, L.** (1998): Symmetric weak-form integral equation method for three-dimensional fracture analysis. *Comput. Meth. Appl. Mech. Engng*, vol. 151, pp. 435-459.

**Murakami, Y.** (1987): *Stress-Intensity Factors Handbook.* Pergamon Press, Oxford.

**Nikishkov, G.P.; Park, J.H.; Atluri, S.N.** (2001): SGBEM-FEM Alternating Method for Analyzing 3D Non-planar Cracks and Their Growth in Structural Components, *CMES: Computer Modeling in Engineerng & Sciences*, vol. 2, no. 3, pp. 401-422.

**Nishioka, T.; Atluri, S.N.** (1983): Analytical solution for embedded elliptical cracks and finite element – alternating method for elliptical surface cracks, subjected to arbitrary loadings. *Eng. Fract. Mech.*, vol. 17, pp. 247-268.

**Okada, H; Kamibeppu, T.** (2005): A virtual crack closure-integral method (VCCM) for three-dimensional crack problems using linear tetrahedral finite elements, *CMES: Computer Modeling in Engineerng & Sciences*, vol. 10, pp. 229-238.

**Vijaykumar, K.; Atluri, S.N.** (1981): An Embedded Elliptical Crack, in an Infinite Solid, Subject to Arbitrary Crack-Face Tractions," *J. Appl. Mech.*, vol. 103, no. 1, pp. 88-96.

**Xu, G.; Ortiz, M.** (1993): A variational boundary integral method for the analysis of 3-D cracks of arbitrary geometry modelled as continuous distribution of dislocation loops. *Int. J. Numer. Meth. Eng.*, vol. 36, pp. 3675-3701.

**Saito, K.; Kuniya, J.** (2001): Mechanochemical model to predict stress corrosion crack growth of stainless steel in high temperature water. *Corrosion Science*, vol. 43, pp. 1751-1766.

**Peng, Q.J.; Kwon, J.; Shoji, T.** (2004): Development of a fundamental crack tip strain rate equation and its application to quantitative prediction of stress corrosion cracking of stainless steels in high temperature oxygenated water. Journal of Nuclear Materials, vol. 324, pp. 52-61.